

DOI: <http://dx.doi.org/10.21123/bsj.2022.6985>

## Fusion Reaction Study of some Selected Halo Systems

Shaimaa A. Abbas<sup>1</sup> 

Noor Adil Mohammed<sup>2</sup> 

Aeshah Ali Hussein<sup>1</sup> 

Sarah M. Obaid<sup>3\*</sup> 

<sup>1</sup>Department of Physics, College of Education for Pure Science (Ibn-Alhaitham), University of Baghdad, Baghdad, Iraq.

<sup>2</sup>Ministry of Education, Directorate General of Education Rusafa3, Baghdad, Iraq

<sup>3</sup>Department of Biomedical Engineering, Al-Mustaqbal University College, Babil, Iraq

\*Corresponding author email: [sarah.mahdi@mustaqbal-college.edu.iq](mailto:sarah.mahdi@mustaqbal-college.edu.iq)

ORCID ID: [shaimaa19750@gmail.com](mailto:shaimaa19750@gmail.com) , [aisha.sataa.1983@gmail.com](mailto:aisha.sataa.1983@gmail.com) , [noorphysics1@gmail.com](mailto:noorphysics1@gmail.com)

Received 29/1/2021, Revised 8/4/2022, Accepted 10/4/2022, Published Online First 20/9/2022  
Published 1/4/2023



This work is licensed under a [Creative Commons Attribution 4.0 International License](https://creativecommons.org/licenses/by/4.0/).

### Abstract:

The challenge in studying fusion reaction when the projectile is neutron or proton rich halo nuclei is the coupling mechanism between the elastic and the breakup channel, therefore the motivation from the present calculations is to estimate the best coupling parameter to introduce the effect of coupled-channels for the calculations of the total cross section of the fusion  $\sigma_{fus}$ , the barrier distribution of the fusion  $D_{fus}$  and the average angular momentum  $\langle L \rangle$  for the systems  ${}^6\text{He}+{}^{206}\text{Pb}$ ,  ${}^8\text{B}+{}^{28}\text{Si}$ ,  ${}^{11}\text{Be}+{}^{209}\text{Bi}$ ,  ${}^{17}\text{F}+{}^{208}\text{Pb}$ ,  ${}^6\text{He}+{}^{238}\text{U}$ ,  ${}^8\text{He}+{}^{197}\text{Au}$  and  ${}^{15}\text{C}+{}^{232}\text{Th}$  using quantum mechanical approach. A quantum Coupled-Channel Calculations are performed using CC code. The predictions of quantum mechanical approach are comparable with the measured data that is available. Above and below the Coulomb barrier, comparison of theoretical calculations of quantum mechanical with the relevant measured data demonstrates good agreement.

**Keywords:** Average angular momentum, Breakup channel, Fusion barrier distribution, Fusion cross section, Halo nuclei.

### Introduction:

Investigation of the mechanisms of the reaction involving the collisions of weakly bound nuclei at the energies near to the barriers which are stable or radioactive is one of the main fields of Low Energy Nuclear Physics (LENP). Comprehensive theoretical and experimental studies have been focused on understanding the various processes that occur in a collision, as well as the significant couplings that exist between them. On this topic, a few global review papers have been written <sup>1</sup>. The breakup channel plays an important role in collisions of the systems that are tightly bound. Transfer channels are essential, particularly for neutron-halo nuclei. The cross sections have large breakup for the systems of the weakly bound have due to their low breakup threshold, and the breakup mechanism has efficient on other reaction channels <sup>2</sup>. The study of such reactions is significant in astrophysics, and several of those reactions could be significant gateways for super-heavy elements production. Fusion is affected by two in a weakly bound projectile collision. firstly, a nature of the

static, the fusion barrier has various property relative to the fusion barrier for the same target for a tightly bound isotope. The barriers are lower due to the longer density tail. At the energies near to the sub-barrier, it is generally thought to contribute to greater fusion cross sections. The dynamic of the elastic channel coupling with inelastic, breakup, and transition channels is the second thing to consider. The bound states inelastic excitations and the channels of the direct transfer have been shown to enhance the cross sections of the fusion at the energies near to sub-barrier. On the contrary, the break-up method has a number of features when it establishes continuum status, and the impact of connections to sources is debatable in the continuum. As the binding is weak, the breakup is still quite wide and the elastic channel is very strongly coupled. Thus, the cross section, along with the normal transfer and inelastic channels, can play a relevant role <sup>3</sup>. The role of the breakup channel has been studied extensively by Majeed and his collaborators and for more details we refer the

readers to refs.<sup>4-8</sup>. Fusion reaction for some light, medium and heavy mass systems using the semiclassical approach seems very competitive to study the fusion reactions properties<sup>9-13</sup>.

The purpose of this work is to employ quantum mechanics by means of the coupled-channels to study the effect of coupling the breakup channel on the theoretical predictions of the total cross section of the fusion  $\sigma_{fus}$ , the barrier distribution of the fusion  $D_{fus}$  and the average angular momentum  $\langle L \rangle$  for the systems  ${}^6\text{He}+{}^{206}\text{Pb}$ ,  ${}^8\text{B}+{}^{28}\text{Si}$ ,  ${}^{11}\text{Be}+{}^{209}\text{Bi}$ ,  ${}^{17}\text{F}+{}^{208}\text{Pb}$ ,  ${}^6\text{He}+{}^{238}\text{U}$ ,  ${}^8\text{He}+{}^{197}\text{Au}$  and  ${}^{15}\text{C}+{}^{232}\text{Th}$ . These systems involving light halo nuclei as a projectile. The calculations were conducted using the CC code. The results are compared with the measured data available. The code that used in the calculations is CC code

### Theoretical Background

#### Fusion cross section

The basic formula for calculating elastic and fusion cross sections is derived using a single-channel potential model. In three dimensions, Schrödinger equation is given<sup>14</sup>:

$$\left[ -\frac{\hbar^2}{2\mu} \nabla^2 + V(r) - E \right] \phi(r) = 0 \quad \dots\dots\dots 1$$

where  $V(r)$  is the complete potential, which is equal to the contribution comes from the nuclear potential and the potential of Coulomb.,  $[V(r) = V_C(r) + V_N(r)]$  and  $\mu$  is the system reduced mass.

The nuclear potential is taken as the Woods-Saxon potential<sup>14</sup>

$$V_n(r) = \frac{-V_0}{1 + \exp\left[\frac{r-R_n}{a_0}\right]} \quad \dots\dots\dots 2$$

where  $V_0$  belongs to the depth of potential and  $a_0$  was the potential diffuseness. The radius  $R_n$  of the nuclear potential was described as with<sup>14</sup>,

$$R_n = r_0 \left[ A_P^{\frac{1}{3}} + A_T^{\frac{1}{3}} \right] \quad \dots\dots\dots 3$$

Where;  $r_0$  is the radius parameter.

This equation can be solved directly in absence of the potential  $v(r)$  in the form  $\phi = \exp(i \vec{k} \cdot \vec{r})$ ,  $\vec{k}$  is the magnitude of the wave number vector is given

by  $k = \sqrt{2\mu E} / \hbar$ . The asymptotic form of this solution<sup>15</sup>

$$\phi(r, \theta) = e^{i\vec{k} \cdot \vec{r}} \rightarrow \frac{i}{2k} \sum_{l=0}^{\infty} (2l+1) i^l \left( \frac{e^{-ik(r-\frac{\pi}{2})}}{r} - \frac{e^{ik(r-\frac{\pi}{2})}}{r} \right) P_l(\cos\theta), r \rightarrow \infty \quad \dots\dots\dots 4$$

where the angle  $\theta$  is between  $\vec{k}$ ,  $\vec{r}$  and  $P_l$  are the polynomials of Legendre. Due to the potential, the solution enhanced in behaviour. Because the potential reaches zero at infinity, the wave-function asymptotic shape can be described similar to Eq. 2. the plane waves will be replacing with the corresponding waves of Coulomb, the form of asymptotic is<sup>16</sup>

$$\phi(r, \theta) \rightarrow \frac{i}{2k} \sum_{l=0}^{\infty} (2l+1) e^l \left( \frac{H_l^{(-)}(kr)}{r} - S_l \frac{H_l^{(+)}(kr)}{r} \right) P_l(\cos\theta), r \rightarrow \infty \quad \dots\dots\dots 5$$

where  $H_l^{(-)}(kr)$  and  $H_l^{(+)}(kr)$  are the waves of Coulomb outgoing and incoming, respectively.  $S_l$  is the S-Matrix for the nuclear is labelled and generally it's a complicated term to be computed. The calculation of the S-matrix is performed by the expansion of the wave function  $\phi(\vec{r})$  with the spherical harmonics as<sup>16</sup>

$$\phi(\vec{r}) = \sum_{l=0}^{\infty} \sum_{m=-l}^l A_{lm} \frac{u_l(r)}{r} Y_{lm}(\hat{r}) \quad \dots\dots\dots 6$$

where  $A_{lm}$  being the expansion of the coefficients for the equation of Schrödinger which are satisfied by  $u_l(r)$  is<sup>17</sup>

$$\left[ -\frac{\hbar^2}{2\mu} \frac{d^2}{dr^2} + V(r) + \frac{l(l+1)\hbar^2}{2\mu r^2} - E \right] u_l(r) = 0 \quad \dots\dots\dots 7$$

The boundary conditions are used to solve this equation.

$$u_l(r) \sim r^{l+1} \quad r \rightarrow 0 \quad \dots\dots\dots 8$$

$$u_l(r) = H_l^{(-)}(kr) - S_l H_l^{(+)}(kr) \quad r \rightarrow \infty \quad \dots\dots\dots 9$$

when  $S_l$  has taken, the elastic cross section of the differential is determined as<sup>17</sup>

$$\frac{d\sigma_{el}}{d\Omega} = |f(\theta)|^2 \quad \dots\dots\dots 10$$

where

$$f(\theta) = \frac{i}{2k} \sum_{l=0}^{\infty} (2l+1) P_l(\cos\theta) (1 - S_l) \quad \dots\dots\dots 11$$

The total elastic cross section can be found as<sup>17</sup>

$$\sigma_{el} = 2\pi \int_{-1}^1 d(\cos\theta) \frac{d\sigma}{d\Omega} = \frac{\pi}{k^2} \sum_{l=0}^{\infty} (2l+1) |S_l - 1|^2 \quad \dots\dots\dots 12$$

Fusion reactions could be considered as incident flow absorption. The s-matrix absolute value is less than unity, when the potentials are complex, i.e.  $|S| < 1$ , and from Eq. 3 It is possible to quantify the difference in total radial flux between the incoming and outgoing waves<sup>18</sup>

$$j_{in} - j_{out} = \frac{\hbar k}{\mu} \frac{\pi}{k^2} \sum_l (2l + 1) (1 - |S_l|^2) \dots\dots\dots 13$$

To derive Eq. 11, for all the values of  $\theta$  to be considered, the radial flux has been integrated and divided by the incident flux,  $\nu = \hbar k/\mu$  the fusion cross section is then taken as<sup>18</sup>

$$\sigma_{fus}(E) = \frac{\pi}{k^2} \sum_l (2l + 1) (1 - |S_l|^2) \dots\dots\dots 14$$

In the heavy-ion fusion, the regular boundary condition at origin is not imposed Eq. 8, IWBC is called the “incoming wave boundary condition” and it has been applied with the goal of preserving the real potential. The wave function has a form under this boundary condition and can be written as<sup>18,19</sup>

$$u_l(r) = T_l \exp\left(-i \int_{r_{abs}}^r k_l(r') dr'\right) \quad r \leq r_{abs} \dots\dots 13$$

at a distance less than radius absorption  $r_{abs}$ , which is considered to be within the barrier of Coulomb.  $k_l(r)$  is number of the local the wave for the  $l$ -th wave partial, which can be described as<sup>18</sup>

$$k_l(r) = \sqrt{\frac{2\mu}{\hbar^2} \left( E - V(r) - \frac{l(l+1)\hbar^2}{2\mu r^2} \right)} \dots\dots 14$$

Due to the occurring of the strong absorption in the region of the interior, the incoming wave boundary condition is equal such that the incoming flux is not returned. The final results for heavy-ion fusion reactions are not really dependent on the radius of absorption  $r_{abs}$  and the minimum position of the potential is also considered. With IWBC,  $T_l$  in Eq. 13 is the coefficient of transmission, therefore the S-matrix,  $S_l$  in Eq.7 is nothing but the coefficient of reflection. So, Eq.14 is turned into<sup>18,20</sup>

$$\sigma_{fus}(E) = \frac{\pi}{k^2} \sum_l (2l + 1) P_l(E) \dots\dots\dots 15$$

where  $P_l(E)$  is called the  $l$ -wave penetrability for the scattering which is described as<sup>19</sup>

$$P_l(E) = 1 - |S_l|^2 = \frac{k_l(r_{abs})}{k} |T_l|^2 \dots\dots\dots 16$$

the boundary conditions included by Eq.6 and Eq.13.

### 2.2 The distribution of the fusion barrier

The classical cross section of the fusion can be written as

$$\sigma_{fus}^{cl}(E) = \pi R_b^2 \left(1 - \frac{V_b}{E}\right) \theta(E - V_b) \dots\dots\dots 17$$

where  $R_b$  is the barrier position and  $V_b$  is the barrier height. The first derivative of the product is noticeable from this expression of the cross-section of the fusion  $\sigma_{fus}^{cl}$  and the energy of the center of mass  $E$ ,  $d\left(\frac{E\sigma_{fus}^{cl}}{dE}\right)$ , is equivalent to the penetrability of classical mechanics for a one-dimension height barrier  $V_b$

$$\frac{d}{dE} [E\sigma_{fus}^{cl}(E)] = \pi R_b^2 \theta(E - V_b) = \pi R_b^2 P_{cl}(E) \dots\dots\dots 18$$

and the delta's function second derivative,

$$\frac{d^2}{dE^2} [E\sigma_{fus}^{cl}(E)] = \pi R_b^2 \delta(E - V_b) \dots\dots\dots 19$$

The effect of tunnelling smears the delta function of quantum mechanics. An analytical formula can be taken for the fusion cross section if an inverse parabola approaches the Coulomb barrier referring to the well-known Wong formula,

$$\sigma_{fus}(E) = R_b^2 \frac{\hbar\Omega}{2E} \ln\left(1 + \exp\left[\frac{2\pi}{\hbar\Omega}(E - V_b)\right]\right) \dots\dots\dots 20$$

where  $\hbar\Omega$  is the barrier of Coulomb curvature. The first order derivative of  $E\sigma_{fus}(E)$  is related to the penetrability as<sup>21</sup>

$$\frac{d}{dE} [E\sigma_{fus}^{cl}(E)] = \frac{\pi R_b^2}{1 + \exp\left[-\frac{2\pi}{\hbar\Omega}(E - V_b)\right]} = \pi R_b^2 P(E) \dots\dots\dots 21$$

This equation directly results in the relationship between the cross section and the first penetrability derivative<sup>21</sup>

$$\frac{d^2}{dE^2} [E\sigma_{fus}^{cl}(E)] = \pi R_b^2 \frac{2\pi}{\hbar\Omega} \frac{e^{-2\pi(E - V_b)/\hbar\Omega}}{(1 + e^{-2\pi(E - V_b)/\hbar\Omega})^2} = \pi R_b^2 \frac{dP(E)}{dE} \dots\dots\dots 22$$

### Results and Discussion:

In this work, the theoretical calculations of the cross-section of fusion  $\sigma_{fus}$ , the distribution barrier  $D_{fus}$  and mean angular momentum  $\langle L \rangle$  using the quantum mechanical approach for the systems  ${}^6\text{He}+{}^{206}\text{Pb}$ ,  ${}^8\text{B}+{}^{28}\text{Si}$ ,  ${}^{11}\text{B}+{}^{209}\text{Bi}$  and  ${}^{17}\text{F}+{}^{208}\text{Pb}$ ,  ${}^6\text{He}+{}^{197}\text{Au}$ ,  ${}^6\text{He}+{}^{238}\text{U}$ ,  ${}^8\text{He}+{}^{197}\text{Au}$  and  ${}^{15}\text{C}+{}^{232}\text{Th}$ . The quantum mechanical calculations using CC code for the  $\sigma_{fus}$ ,  $D_{fus}$  and  $\langle L \rangle$  are compared with measured data. The parameters of the potential (Woods-Saxon potential) with different parametrizations which is called Winther-Akyüz potential used throughout in the current calculations are illustrated in Table 1. These parameters were obtained by the least-square fit method to match the correct position of the experimental barrier height+ at the center point.

**Table 1. Winther-Akyüz potential parameters with barrier height  $V_b$** 

Projectile +Target	$V_0$ (MeV)	$a_0$ (fm)	$r_0$ (fm)	$V_b$ (MeV)
${}^6\text{He}+{}^{206}\text{Pb}$	-131.9	0.6	1.2	18.66
${}^8\text{B}+{}^{28}\text{Si}$	-96.9	0.6	1.1	11.45
${}^{11}\text{B}+{}^{209}\text{Bi}$	-191	0.898	1.001	37.86
${}^{17}\text{F}+{}^{208}\text{Pb}$	-115.5	0.83	1.09	86.59
${}^6\text{He}+{}^{197}\text{Au}$	-192.9	0.7	1.1	18.13
${}^6\text{He}+{}^{238}\text{U}$	-76.0	0.816	1.192	19.60
${}^8\text{He}+{}^{197}\text{Au}$	-162.3	0.850	1.03	17.71
${}^{15}\text{C}+{}^{232}\text{Th}$	-134.0	0.8	1.1	60.41

The results of the quantum mechanical calculations show in Fig. 1 in the panels (a, b, c) for  $\sigma_{fus}$ ,  $D_{fus}$  and  $\langle L \rangle$ , respectively, for the system  ${}^6\text{He}+{}^{206}\text{Pb}$ . The results show that the coupling calculations and non-coupling channels were able to describe the measured data below and around Coulomb barrier  $V_b$ . The calculations and measured data <sup>22</sup> in all figures are plotted in both logarithm and linear scales for  $\sigma_{fus}$  (mb). The calculations enhanced markedly below the Coulomb when the coupling channel were included. For this system the average angular momentum  $\langle L \rangle$  agrees well with the measured data for both coupling and 30.8/\*without coupling.

Fig.2 (a, b and c) depicted the comparison of theory and measured data of  $\sigma_{fus}$ ,  $D_{fus}$  and  $\langle L \rangle$  with the measured data for the system  ${}^8\text{B}+{}^{28}\text{Si}$ . The measured data are taken from<sup>23</sup>. Our results of  $\sigma_{fus}$  for both coupling and no coupling channels reproduce the measured data, whereas the linear curves for coupling and no coupling channels results overshoot the measured data. The results of our calculations for  $D_{fus}$ , the coupling channel predictions agreed more reasonably with experimental data <sup>22</sup>, while the results of the mean angular momentum  $\langle L \rangle$  overshoots the measured data above the Coulomb barrier, for both coupling and no-coupling. Fig.3 panel (a), (b) and (c) compared theoretical results with measured data for  $\sigma_{fus}$ ,  $D_{fus}$  and  $\langle L \rangle$  for the system  ${}^{11}\text{Be}+{}^{209}\text{Bi}$ . The calculations of  $\sigma_{fus}$  both logarithmic and linear curves for coupling and no coupling channels results overshoot the measured data<sup>24</sup>. The results of the calculations with channel coupling are in agreed more with the measured data for the  $D_{fus}$ , while the coupling channel result for average angular momentum  $\langle L \rangle$  agrees with the measured data above the barrier. Fig.4 depicts the comparison of the calculated  $\sigma_{fus}$ ,  $D_{fus}$  and  $\langle L \rangle$  with their corresponding measured data for both coupling and no coupling for the system  ${}^{17}\text{F}+{}^{208}\text{pb}$ . The

calculations of  $\sigma_{fus}$  for both coupling and non-coupling could not describe two experimental data<sup>25</sup> below the Coulomb barrier  $V_b$ , because  ${}^{17}\text{F}$  is proton rich halo nucleus that made suppression to the fusion cross section which makes theoretical predictions overshoots the measured data. Including the coupling in the calculations of  $D_{fus}$  reproduce the behaviour of the experimental data and deviate from the Gaussian shape in the case of no coupling. The calculations with coupling included for  $\langle L \rangle$  agrees with experiment above  $V_b$  and overshoots the experimental values below  $V_b$ . Fig.5 panel (a), (b) and (c) show the results of the quantum mechanical calculations for  $\sigma_{fus}$ ,  $D_{fus}$  and  $\langle L \rangle$ , respectively, for the system  ${}^6\text{He}+{}^{238}\text{U}$  compared to the experimental data<sup>25</sup>. The results show that calculations included coupling and no-coupling channels were able to describe the measured data below and around Coulomb barrier  $V_b$ .

The inclusion of the coupled channel enhances the calculations of  $\sigma_{fus}$  below the Coulomb barrier. While  $D_{fus}$  and  $\langle L \rangle$  calculations with shows ripple behaviour with two peaks appear for  $D_{fus}$  which are closer to the experimental data. Fig.6 panel (a), (b) and (c) presented the theoretical predictions compared to measured data <sup>26</sup> for  $\sigma_{fus}$ ,  $D_{fus}$  and  $\langle L \rangle$  for the system  ${}^8\text{He}+{}^{197}\text{Au}$ . The location of barrier of the measured data for Coulomb  $V_b$  appear as an arrow on the  $E_{c.m.}$  axis. For this system the inclusion of the coupling has very slight effect on the peak height of the  $D_{fus}$  calculations and have same results in the case of no-coupling and in general have no agreement with the experimental data for the  $\sigma_{fus}$  and  $\langle L \rangle$  calculations expect very slightly difference in the peak value of  $D_{fus}$ .

The calculated results of  $\sigma_{fus}$ ,  $D_{fus}$  and  $\langle L \rangle$  were compared with the measured data<sup>27</sup> in panels (a), (b) and (c) of Fig.7, respectively for  ${}^{15}\text{C}+{}^{232}\text{Th}$  system. The inclusion of coupled channel in quantum mechanical calculations enhanced markedly the calculations for the  $\sigma_{fus}$  below the Coulomb barrier makes theoretical predictions in more match with the measured data and were able to reproduce the data satisfactorily. The quantum mechanical with and without coupling couldn't describe the experimental data for the  $D_{fus}$  and  $\langle L \rangle$ . The results of the calculations for fusion cross section  $\sigma_{fus}$  for both coupling and no-coupling channels agreed with the measured data in both logarithmic and linear curves. The results of the calculations for  $D_{fus}$  the coupling channel results overshoot the measured data for this reaction. For mean angular momentum  $\langle L \rangle$  the coupling channel

results overshoot the measured data below the Coulomb barrier. But we found good agreement with the measured data above this barrier. The results from the present study agree with previous work of Hamid and Majeed<sup>28</sup>, for the calculations of

the fusion cross section and the fusion barrier distribution where they had employed quantum mechanical model based on the continuum discretized coupled-channel method to study some systems involving weakly bound nuclei.

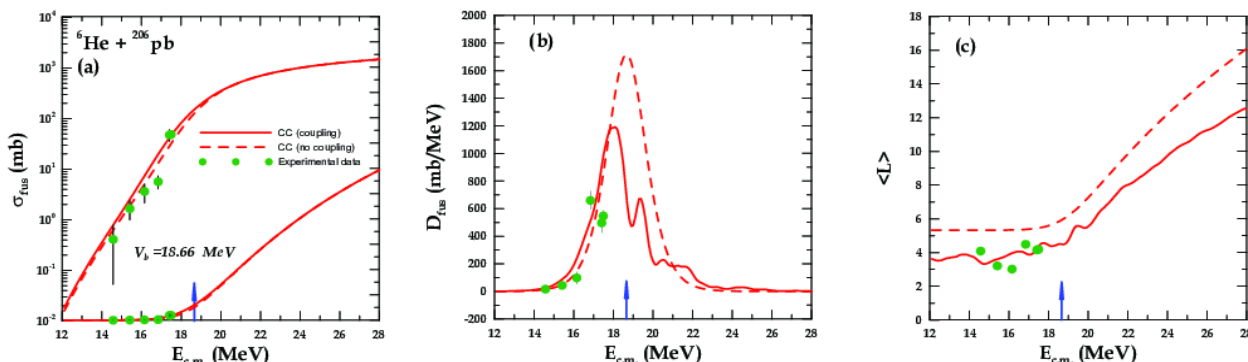


Figure 1. Displays theoretical predicted for the  $\sigma_{fus}$ , and  $D_{fus}$ ,  $\langle L \rangle$  compared to measured data<sup>22</sup> for  ${}^6\text{He}+{}^{206}\text{Pb}$  system.

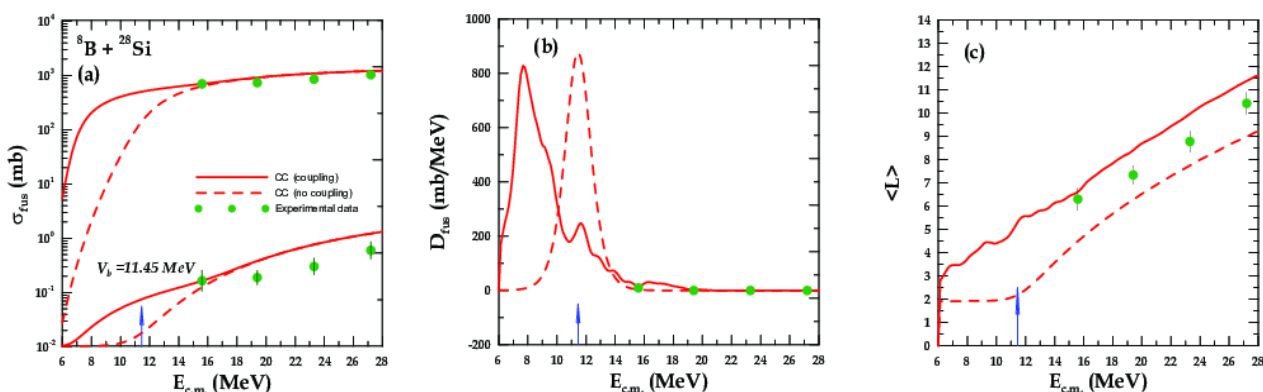


Figure 2. Displays theoretical predicted for the  $\sigma_{fus}$ , and  $D_{fus}$ ,  $\langle L \rangle$  compared to measured data<sup>23</sup> for  ${}^8\text{B}+{}^{28}\text{Si}$  system.

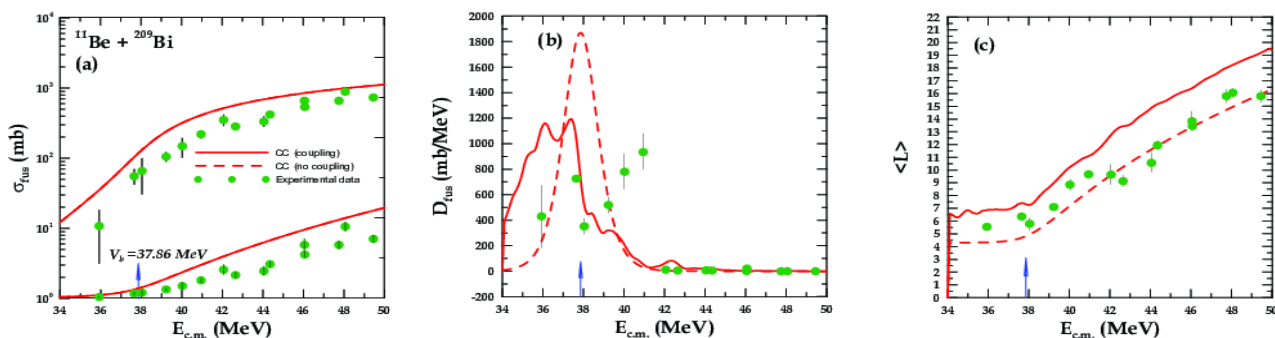


Figure 3. Displays theoretical predicted for the  $\sigma_{fus}$ , and  $D_{fus}$ ,  $\langle L \rangle$  compared to measured data<sup>24</sup> for  ${}^{11}\text{Be}+{}^{209}\text{Bi}$  system.

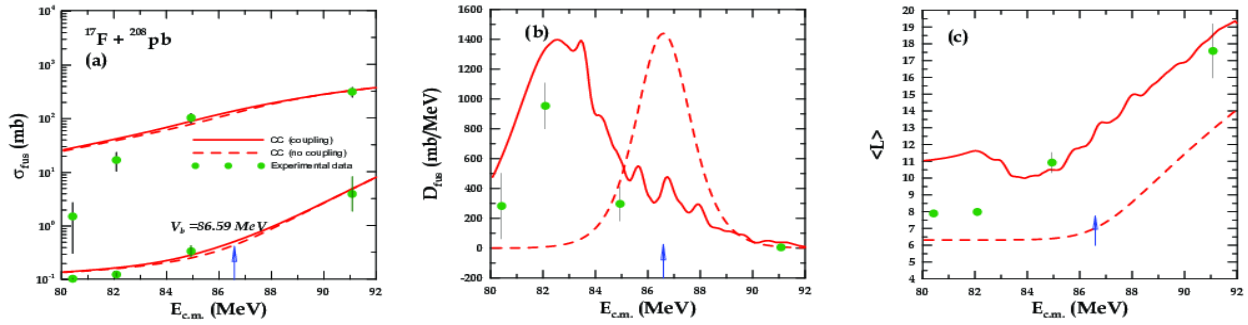


Figure 4. Displays theoretical predicted for the  $\sigma_{fus}$ , and  $D_{fus}$ ,  $\langle L \rangle$  compared to measured data <sup>25</sup> for  $^{17}\text{F}+^{208}\text{pb}$  system.

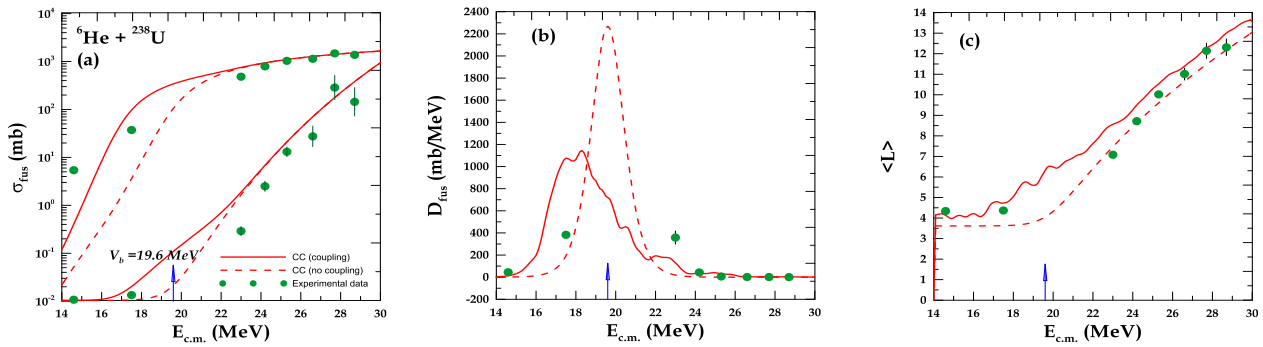


Figure 5. Displays theoretical predicted for the  $\sigma_{fus}$ , and  $D_{fus}$ ,  $\langle L \rangle$  compared to measured data <sup>25</sup>  $\text{He}+^{238}\text{U}$  system.<sup>6</sup>for

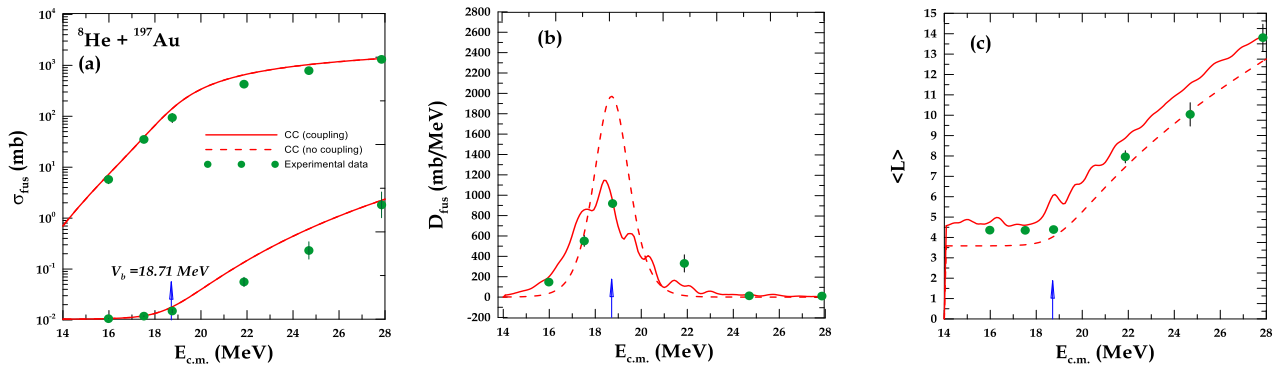


Figure 6. Displays theoretical predicted for the  $\sigma_{fus}$ , and  $D_{fus}$ ,  $\langle L \rangle$  compared to measured data <sup>26</sup> for  $^8\text{He}+^{197}\text{Au}$  system.

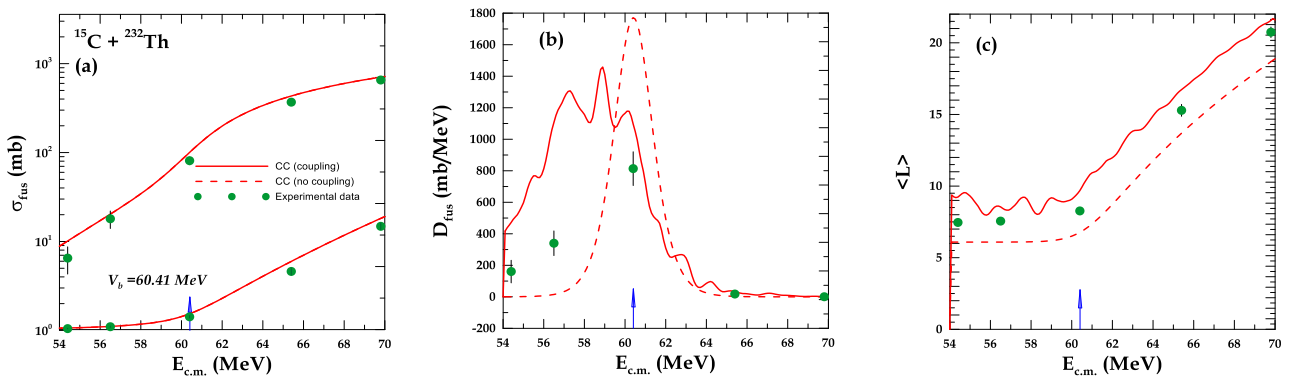


Figure 7. Displays theoretical predicted for the  $\sigma_{fus}$ , and  $D_{fus}$ ,  $\langle L \rangle$  compared to measured data <sup>27</sup> for  $^{15}\text{C}+^{232}\text{Th}$  system.

## Conclusion:

The conducted study detailed theoretical investigation of the calculations for  $\sigma_{fus}$ ,  $D_{fus}$  and  $t \langle L \rangle$  for the systems  ${}^6\text{He}+{}^{206}\text{Pb}$ ,  ${}^8\text{B}+{}^{28}\text{Si}$ ,  ${}^{11}\text{Be}+{}^{209}\text{Bi}$ ,  ${}^{17}\text{F}+{}^{208}\text{Pb}$ ,  ${}^6\text{He}+{}^{238}\text{U}$ ,  ${}^8\text{He}+{}^{197}\text{Au}$  and  ${}^{15}\text{C}+{}^{232}\text{Th}$  were analyzed and discussed. The best fitted coupling parameters were obtained based on the best fitted parameters of the Woods-Saxon parameters that match the centroid of the measured and calculated barrier height  $V_b$ . The results compared to experiment reveals that the breakup channel is very necessary to describe  $\sigma_{fus}$ ,  $D_{fus}$ , and  $\langle L \rangle$  for these systems involving light halo nuclei as a projectile. A comparison of our theoretical calculations of quantum mechanical with the measured data display a reasonable agreement with the available measured data. The results of this study are very important for researchers who are interested in studying the physics of weakly bound systems where the projectile is a halo nucleus.

## Acknowledgements:

Authors acknowledge the financial support from Al-Mustaqbal University College.

## Authors' declaration:

- Conflicts of Interest: None.
- We hereby confirm that all the Figures and Tables in the manuscript are mine ours. Besides, the Figures and images, which are not mine ours, have been given the permission for re-publication attached with the manuscript.
- Ethical Clearance: The project was approved by the local ethical committee in Al-Mustaqbal University College.

## Authors' contributions statement:

Title of manuscript:

S. A. A.: Performed theoretical calculations and wrote the theoretical section.

A. A. H.: Collect the experimental data and arrange it in tables to be used in grapher for comparison with theory.

N. A. M.: Wrote the introduction section with literature review and the goal of the study and participate in writing the result section.

S. M. O.: Contribute in plotting the graphs to compare theory with experiment and wrote the conclusion section and arrange references according to journal author guidelines.

The tables and figures are all original and configured well in all the manuscript.

## References:

1. Pakou A, Sgouros O, Soukeras V, Casal J, Rusek K. Reaction mechanisms of the weakly bound nuclei  ${}^{6,7}\text{Li}$  and  ${}^{7,9}\text{Be}$  on light targets at near barrier energies, Eur Phys J A. 2022 Jan; 58(8): 8-58.
2. Gomes PRS, Mendes Junior DR, Canto LF, Lubian J, de Faria PN. Reduction Methods for Total Reaction Cross Sections. Few-Body Syst. 2016 Mar; 57: 205–216.
3. Majeed FA, The role of the breakup channel on the fusion reaction of light and weakly bound nuclei, Int J Nucl Energ Sci Tech . 2017 Nov; 11: 218-228.
4. Majeed FA, Abdul-Hussien YA, Semiclassical treatment of fusion and breakup processes of  ${}^{6,8}\text{He}$  halo nuclei J Theor App Phys. 2016 Feb; 10: 107-112.
5. Majeed FA, Hamodi RSh, Hussian FM. Effect of coupled channels on semiclassical and quantum mechanical calculations for heavy ion fusion reactions, J ComputTheor Nanosc.2017 May; 14: 2242-2247.
6. Majeed FA, AlAteah KHH, Mehemed MS. Coupled channel calculations using semi-classical and quantum mechanical approaches for light and medium mass systems, Int J Energ Sci Tech. 2018 Mar; 11: 291-308.
7. Majeed FA, Mahdi FA. Quantum Mechanical Calculations of a Fusion Reaction for Some Selected Halo Systems Ukran J Phys. 2019 Jan; 64: 11-18.
8. Majeed FA, Abdul-Hussien YA, Hussian FM. Fusion Reaction of Weakly Bound Nuclei, IntechOpen. 2019.
9. Najim AJ, Majeed FA, and Al-Attayah KH. Improved calculation of fusion barrier distribution IOP Conf Ser: Mat Sci Eng. 2019Apr; 571: 012124.
10. Najim AJ, Majeed FA, Al-Attayah KH. Coupled-channel calculations for fusion reactions of  ${}^6\text{Li}+{}^{64}\text{Ni}$ ,  ${}^{40}\text{Ca}+{}^{96}\text{Zr}$  and  ${}^{124}\text{Sn}+{}^{48}\text{Ca}$  Systems, J Eng Appl Sci. 2019 Jul; 14: 10406.
11. Musa HJ, Majeed FA, Mohi AT. Coupled channels calculations of fusion reactions for  ${}^{46}\text{Ti}+{}^{64}\text{Ni}$ ,  ${}^{40}\text{Ca}+{}^{194}\text{Pt}$  and  ${}^{40}\text{Ar}+{}^{148}\text{Sm}$  systems. Iraqi J Phys. 2020 Dec; 18: 84.
12. Musa HJ, Majeed FA, Mohi AT. Improved WKB Approximation for Nuclear Fusion Reactions, IOP Conf Ser: Mat Sci Eng. 2020 Feb; 871: 012063.
13. Mehemed MS, Obaid SM, Majeed FA. Coupled channels calculation of fusion reaction for selected medium systems, Int J Nucl Ener Sci Tech. 2020 Dec; 14: 165.
14. Canto LF, Gomes PRS, Donangelo R, Hussein MS. Fusion and breakup of weakly bound nuclei Phys Rep. 2006 Feb; 424: 1-111.
15. Griffiths DJ. Introduction to Quantum Mechanics. Wiley-VCH; 2nd edition, 2004.
16. Sakurai JJ, Napolitano J. Modern Quantum Mechanics. Cambridge University Press; 3rd edition, 2020.
17. Walecka JD, Theoretical Nuclear and Subnuclear Physics, World Scientific Publishing Co Pte Ltd, 2004.

18. Yang J, Study of one-neutron halo through (d, p) transfer reactions. Ph.D. Thesis, Arenberg Doctoral School- KU Leuven, 2019.
19. Alqobory RAA. Evaluation of the Compton (Incoherent) and Rayleigh (Coherent) Differential Cross Sections of Scattering for Rhodium 103Rh45 and Tantalum<sup>181</sup>Ta<sub>73</sub> by Employing CSC model. Baghdad Sci J. 2012 Sep; 9(3):554-558.
20. Abdullah AM, Salloum AD. Comparison Between the Theoretical Cross Section Based on the Partial Level Density Formulae Calculated by the Exciton Model with the Experimental Data for <sup>197</sup>Au<sub>79</sub> nucleus. Baghdad Sci. J. 2020 Mar; 18(1):139-143.
21. Yusa S, Hagino K, Rowley N. Role of noncollective excitations in heavy-ion fusion reactions and quasi-elastic scattering around the Coulomb barrier. Phys Rev C. 2012 May, 85: 054601.
22. Jiang CL, Back BB, Rehm KE, Hagino K, Montagnoli KG, Stefanini AM. Heavy-ion fusion reactions at extreme sub-barrier energies. Eur Phys J A. 2021 Jul; 57: 235: 1-47.
23. Dasso CH, Pollarolo G. Macroscopic formfactors for pair transfer in heavy ion reactions, Phys Lett B. 1985 May ;155: 223.
24. Wolski R, Martel I, Acosta L, Aguado J, Angulo C, Berjillos R, et al. Sub-barrier fusion of <sup>6</sup>He with <sup>206</sup>Pb, Euro Phys A. 2011Sep; 47: 111.
25. Rehm KE, Esbensen H, Jiang CL, Back B B, Borasi F, Harss B, et al. Fusion Cross Sections for the Proton Drip Line Nucleus <sup>17</sup>F at Energies below the Coulomb Barrier. Phys Rev Lett. 1998 Oct; 81: 334.
26. Penionzhkevich Yu E , Astabatyana RA, Demekhina NA, Gulbekian GG, Kalpakchieva R , KulkoAA, Lukyanov SM, et al. . Excitation functions of fusion reactions and neutron transfer in the interaction of <sup>6</sup>He with <sup>197</sup>Au and <sup>206</sup>Pb. Eur Phys J A 2007Jun; 31:185-194.
27. Alcorta M, Rehm KE, Back B B, Bedoor S, Bertone PF, Deibel CM, et al. Fusion Reactions with the One-Neutron Halo Nucleus <sup>15</sup>C. Phys. Rev. Lett. 2011Apr;106:172701.
28. Mahdi M H A, Majeed FA, Fusion reaction study of halo system by quantum mechanical-based model for <sup>6</sup>He+<sup>64</sup>Zn, <sup>8</sup>B+<sup>58</sup>Ni and <sup>8</sup>He+<sup>197</sup>Au systems. Bull Pol Acad Sci Tech Sci 2021 Aug; 69(4): e137734,

## دراسة الاندماج النووي لبعض النوى الهالوية

سارة مهدي عبيد<sup>3</sup>نور عادل محمد<sup>2</sup>عائشة علي حسين<sup>1</sup>شيماء أكرم عباس<sup>1</sup>

<sup>1</sup> قسم الفيزياء، كلية التربية للعلوم الصرفة (أبن-الهيثم)، جامعة بغداد، بغداد، العراق  
<sup>2</sup> وزارة التربية، المديرية العامة لتربية الرصافة الثالثة، بغداد، العراق  
<sup>3</sup> قسم هندسة الطب الحيوي، كلية المستقبل الجامعة، بابل، العراق

### الخلاصة:

التحدي في دراسة تفاعل الاندماج عندما تكون القذيفة عبارة عن نوى هالة غنية بالنيوترونات أو البروتونات هو آلية الاقتران بين القناة المرنة وقناة التفكك ، وبالتالي فإن الدافع من الحسابات الحالية هو تقدير أفضل معلمة اقتران لإدخال تأثير القنوات المقترنة لحساب مقطع الاندماج الكلي  $\sigma_{fus}$  وحاجز توزيع الاندماج  $D_{fus}$  و متوسط الزخم الزاوي  $\langle L \rangle$  للأنظمة <sup>6</sup>He+<sup>206</sup>Pb, <sup>8</sup>B+<sup>28</sup>Si, <sup>11</sup>Be+<sup>209</sup>Bi, باستخدام مقاربة الميكانيك الكمي. أنجزت الحسابات بإستعمال البرنامج الحاسوبي CC. قورنت الحسابات لمقطع الاندماج الكلي الميكانيك الكمي مع البيانات العملية المتوفرة لكل نظام، وجدَ إن حسابات قنوات الإقتران للميكانيك الكمي في توافق أكثر مع البيانات العملية.

**الكلمات المفتاحية:** متوسط الزخم الزاوي، قناة التفكك، توزيع حاجز الاندماج ، مقطع أستطارة الاندماج، أنظمة نوى الهالة.